Characteristics of Orifice Jets at Low Reynolds Numbers

Seyed Sobhan Aleyasin[1] and Mark Francis Tachie[1]

[1]*University of Manitoba, Winnipeg, MB, Canada, R3T 5V6*
Mark.Tachie@umanitoba.ca

Abstract - An experimental study was undertaken to investigate the effects of nozzle geometries on the mixing characteristics and turbulent transport phenomena in the near region of free orifice jets at a low Reynolds number. The cross-sections examined were round, and ellipses with aspect ratio 2 and 3. For each orifice cross-section, detailed velocity measurements were made at a Reynolds number of 2500 using a particle image velocimetry. It was observed that, regardless of aspect ratio of the elliptic nozzles, the behavior of the jets were different in the major and minor planes. The width of the jet in the major plane initially decreased before starting to grow while in minor planes the width increased monotonically from the exit. The results showed that the elliptic nozzle with aspect ratio 3 had the highest spread rate. Two-point correlations were employed to estimate the size and shape of turbulent structures in the jets. The results show that the size of structures increased with streamwise distance from the jet exit.
Keywords: Turbulent jet, axis-switching, orifice nozzles and low Reynolds number

1. Introduction

Turbulent jets have been the subject of numerous investigations because of their diverse engineering and industrial applications including combustion, chemical processes, heating, ventilating and air conditioning. It is generally acknowledged that initial conditions such as exit Reynolds number, turbulence intensity, nozzle-exit geometry and nozzle type have significant impacts on the mixing performance and turbulence characteristics of jets [1]. Mi et al. [2] examined the effects of nozzle type on the mixing characteristics of round turbulent jets at Reynolds number, Re = 16000. They reported that among three types of round turbulent jets, the largest rate of mixing with ambient fluid corresponded to the jet issuing from sharp-edged orifice followed by the jet produced from contoured nozzle, and the least effective mixing occurred when the jet was produced from a pipe. The experimental results on round jets presented by Quinn [3] also showed that, even at Re = 184000, jets produced from orifice nozzle had higher mixing compared to those from contoured nozzle. Abdel-Rahman et al. [4] investigated the effect of Reynolds number on the near field region of a smooth contraction round turbulent air jet. The measurements were conducted in the near field region and the Reynolds number was varied from 1400 to 20000. They observed that the centerline velocity decayed faster and the potential core became shorter with decreasing Reynolds number which led to better mixing with the ambient fluid.

Over the last few decades, considerable research efforts have been made to advance understanding of turbulent jets produced from noncircular nozzles mainly due to their superior mixing characteristics compared to round jets. However, most of these investigations were performed at relatively high Reynolds number (8000 – 184000) [5,6]. For example, Quinn [6] compared jets produced from two types of triangular nozzle (isosceles and equilateral) with a round nozzle at Re = 184000. It was observed that the fastest mixing occurred in the equilateral triangular jet while the least mixing was observed in the round jet. Mi et al. [7] studied turbulent jets issuing from various nozzle geometries (square, rectangular and ellipse with aspect ratio 2, star, cross, isosceles and equilateral triangles and round) and reported that, in general, the centerline mean velocity of the noncircular jets decayed faster than observed in the round jet, suggesting a higher entrainment of ambient fluid in the case of noncircular jets. The superior mixing properties observed in these noncircular jets compared to round jets have been attributed to axis-switching.

Although turbulent transport and mixing characteristics in the near field region are of great importance in diverse thermo-fluid systems, and the acute sensitivity of the flow dynamics in the near field region to initial conditions such as Reynolds number and nozzle geometry, most of the previous investigations on

turbulent jets were performed in the far field of contoured round and plane jets, and at high Reynolds numbers. The objective of the present study is to investigate the behavior of the near field of turbulent jets produced from different orifice nozzles at a low Reynolds number. Towards this end, experiments were performed to critically examine the near-field characteristics of turbulent round (RD) and elliptic orifice nozzles at a low Reynolds number of 2500. Two different elliptic nozzles with aspect ratios of 2 (ELP2) and 3 (ELP3), but with the same equivalent diameters as the RD nozzle were used to also examine the effect of aspect ratio on the mixing performance.

2. Experimental Procedure

The experiments were conducted in a recirculating open water channel which was 2500 mm long, 200 mm wide and 200 mm deep. The channel was made from transparent acrylic material to facilitate optical access. The jets were produced from the following sharp-edged orifice nozzles: round (RD), ellipse with aspect ratio 2 (ELP2), and ellipse with aspect ratio 3 (ELP3). To facilitate comparison of the different jets, the equivalent diameter of the elliptic nozzles were chosen to match the round nozzle's diameter which was d = 9mm. For each nozzle geometry, measurements were performed at a Reynolds number of Re = 2500, where $Re = U_{max}d/\nu$ and U_{max} is the maximum velocity.

The Cartesian coordinate system was adopted in this study: the streamwise and transverse directions are denoted by x and y, respectively; x = 0 corresponds to the jet exit, y = 0 corresponds to the jet centerline. The experiments were conducted in a plane that extended from the jet exit up to x/d = 7.5, which covered the near field region. As ellipses are asymmetry geometries, the measurements in these jets were made in both their minor and major planes.

A particle image velocimetry (PIV) system was employed to conduct detailed velocity measurements in the symmetry planes of jets. The flow was seeded with silver coated hollow glass spheres of mean diameter 10 μm and specific gravity of 1.1. An Nd-YAG double-pulsed laser that emits green light up to a maximum of 120 mJ/pulse at λ = 532 nm was used to illuminate the flow. The laser sheet was located at the mid-span of the channel, and the flow field was imaged using a high resolution 12 bit 2048 x 2048 pixel charge coupled device camera with a 7.4 μm pixel pitch. Based on convergence tests the mean velocity and higher order turbulent statistics reported in this study were acquired using 6000 instantaneous images and a field of view of 72 mm × 72 mm.

The instantaneous images were post-processed using adaptive correlation of DynamicStudio which is a commercial software developed by Dantec Dynamics Inc. The adaptive correlation uses a multi-pass fast Fourier transform cross-correlation algorithm to determine the average particle displacement within an interrogation area. An interrogation area size of 32 × 32 pixels with 50% overlap was employed to process the instantaneous velocity data. During data acquisition, the PIV parameters were optimized to satisfy the condition that the maximum particle displacement is less than one-quarter of the interrogation area used.

3. Results and Discussion

The non-dimensional contour plots of streamwise mean velocity ($U^* = U/U_{max}$) and Reynolds shear stress ($-uv^* = -uv/U_{max}^2$) for the round and both minor and major planes of the ELP3 are shown in Figure 1. In this and subsequent figures, the velocities and distances are made dimensionless by U_{max} and d respectively. For example, X* denotes x/d and Y* represents y/d. The mean velocity contours show that, shortly after jet exit, the flow accelerates and reaches the highest magnitude due to the vena contracta effect. From Figure 1a, it can be observed that except for an initial portion in which the velocity decay and spread are relatively small, the round jet exhibits almost a linear growth. As the elliptic nozzle is asymmetric, the flow characteristics in the major plane are different from those along the minor plane. For example, the jet width in the direction of the major axis (Figure 1e) initially shrinks before it starts to grow while a monotonic growth can be observed in the minor plane (Figure 1c). As a result, an axis-switching occurs at X* ≈ 2.45.

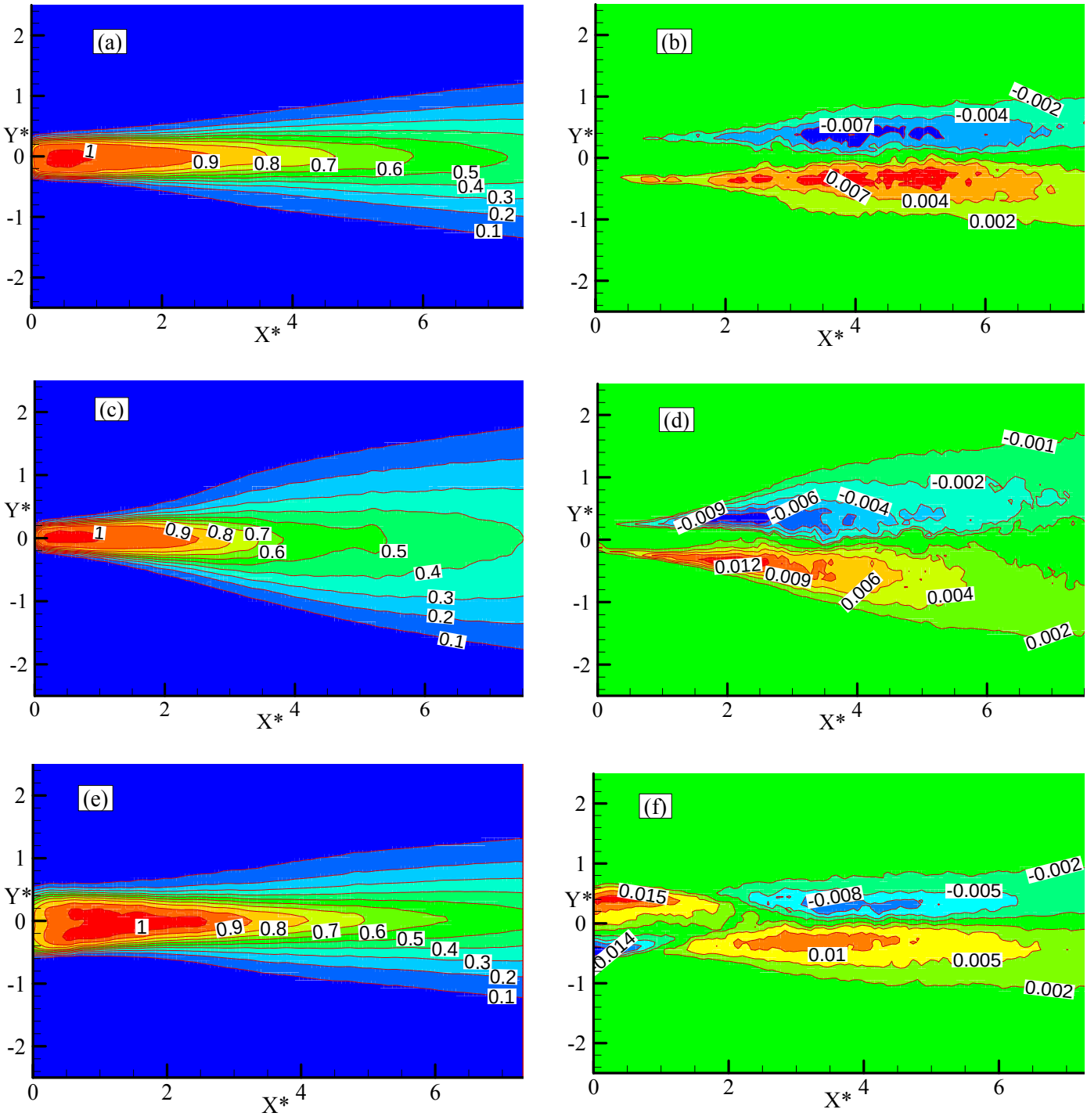

Figure 1: Dimensionless contours of mean streamwise velocity (left column) and Reynolds shear stress (right column). RD (a and b), ELP3_minor (c and d), ELP3_major (e and f).

The Reynolds shear stress contours for both RD (Figure 1b) and ELP3 in minor plane (Figure 1d) show positive and negative values in the bottom and top shear layers respectively. Near the jet exit in the major plane (Figure 1f), however, the region of negative shear stress is observed in the lower shear layer while the shear stress in upper shear layer is positive. Contours of ELP2 (not shown) reveal similar behaviors; however, the location of axis-switching was different from ELP3.

Figure 2 presents dimensionless streamwise turbulence intensity ($u^*_{rms} = u_{rms}/U_{max}$) and transverse turbulence intensity ($v^*_{rms} = v_{rms}/U_{max}$). Near the jet exits, the streamwise turbulence intensity contours exhibit higher values at the interface of shear layers with ambient fluid as the Kelvin-Hemholtz instability initially affects at the interface of jets with ambient fluids. It should be noted that the highest streamwise intensity occurred in the major plane. From the transverse turbulence intensity contours, it can be concluded that the levels of v^*_{rms} are lower compared to u^*_{rms}. Also near the jet exit at the interface of turbulent/ non-turbulent flows, the magnitude of v^*_{rms} is higher compared to the center. This means that the double-peak behavior occurs in this part of the jets; however further downstream the instability enters to the center portion leads to increase of v^*_{rms} around the centerline.

The distributions of mean streamwise velocity decay on the jet centerline and the half-velocity width ($y_{0.5}$/d) are shown in Figure 3. The velocity profiles are quite similar. The decay rate can be obtained using the following equation:

$$\frac{U_{max}}{U_{cl}} = K\left(\frac{X-X_0}{d}\right) \quad (1)$$

Here K is the decay rate and X_0 is the virtual origin of the jet. By employing equation (1), the decay rate of RD, ELP2 and ELP3 within the range of 3 < X* < 7.25 are 0.208, 0.206 and 0.206 respectively. These values are consistent with previous results. For example, Mi et al. [8] reported decay rate of 0.208 and 0.202 for RD and ELP2 at a Reynolds number of 15000; however these values were obtained using data within the streamwise ranges of 11 < X* < 40 and 8 < X* < 40, respectively.

From Figure 3b it can be observed that the width of the RD increased gradually from the exit. For elliptic jets the locations of axis-switching points (where the half-velocity widths in both major and minor planes are identical) are found to be X* = 1.75 and X* = 2.45, respectively, for ELP2 and ELP3. Upstream of the axis-switching points, the width of the jets in the major plane decreases while it grows in the minor plane (but at different rate than the RD) as observed in contour plots. Downstream of the switchover points, the shear layer of all jets increase monotonically; however the growth rates are not the same. Within the range of 3 < X* < 7.25 the spread rates of ELP2_minor, ELP2_major, ELP3_minor and ELP3_major nozzles are 0.167, 0.098, 0.181 and 0.098 respectively. To facilitate comparison of the elliptic nozzles' spread rate with RD, the equivalent width, $y_{0.5\,Eq} = \sqrt{y_{0.5\,minor} \times y_{0.5\,major}}$, is used. The results revealed that ELP3_Eq, ELP2_Eq and RD grow at the rate of 0.134, 0.129 and 0.101, which implies that ELP3 has the highest spreading rate (32% and 4% faster than RD and ELP2, respectively).

Figure 4 shows selected lateral profiles of dimensionless streamwise mean velocity, streamwise turbulence intensity, transverse turbulence intensity and Reynolds shear stresses at three different streamwise distances from the jet exit. Figure 4a exhibits a gradual development of mean streamwise velocity; at X* = 1 the velocity is the highest but confined to a narrow region, Y*≤ 0.5. Further downstream (X* = 7) the profiles become smoother with peak value of $U/U_{mean} \approx 0.5$ and width of 1.5d. From Figure 4b and c, it can be concluded that near the jet exit, the streamwise turbulence intensities are larger than the transverse turbulence intensities regardless of nozzle shape; however their magnitudes become almost similar farther downstream (X* = 7). Furthermore the streamwise and transverse turbulence intensities are highest in the major plane of ELP3. All the turbulence intensities have a double-peak profile initially**,** and evolve into a bell-shaped distribution downstream. The effect of axis-switching is noticeable in Reynolds shear stress profiles (Figure 4d); as there is a sign change near the symmetry lines in the major plane of both ELP2 and ELP3 (at X* = 1 the values are negative while at X* = 3 they are positive).

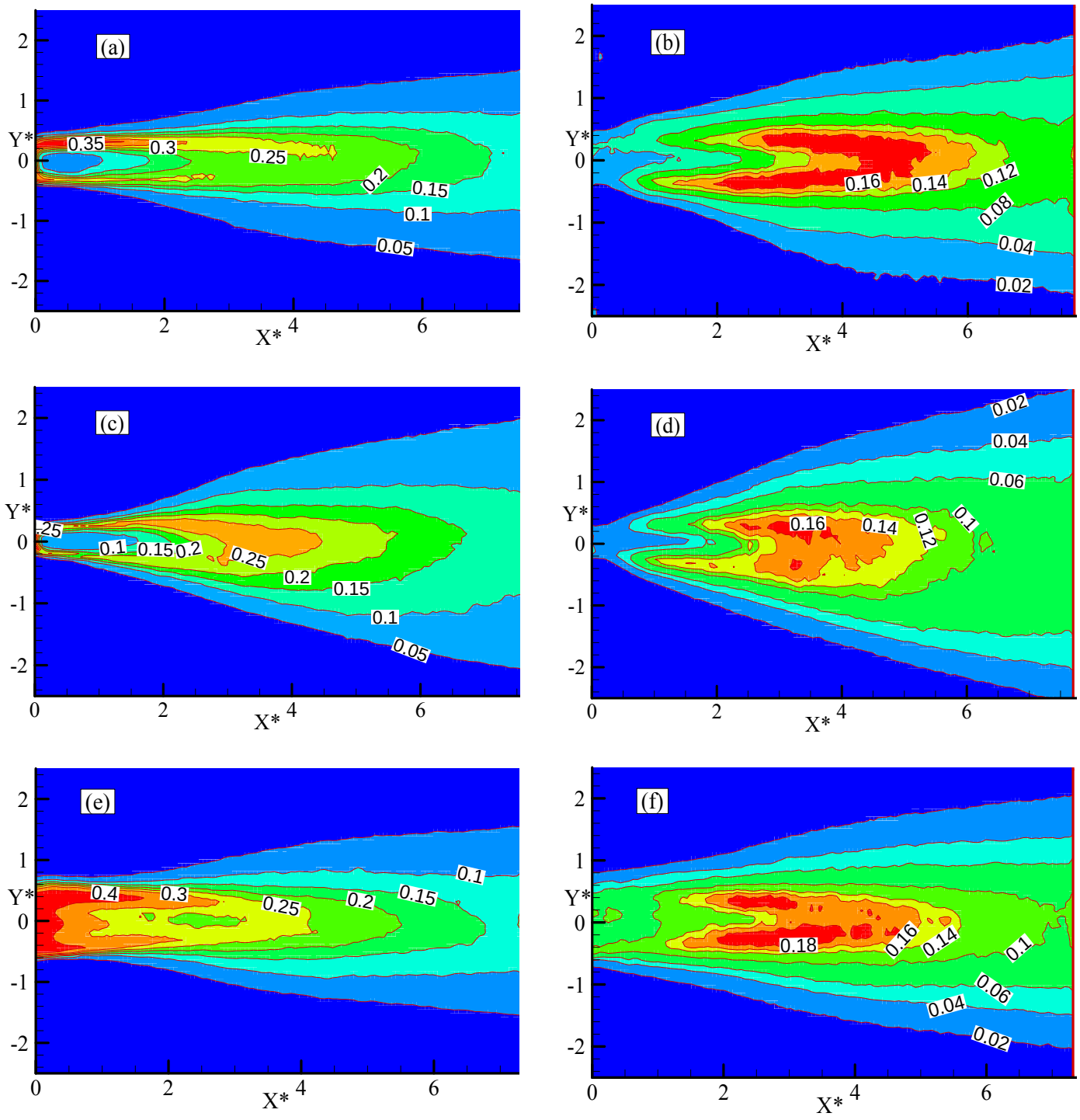

Figure 2: Dimensionless contours of streamwise turbulence intensity (left column) and transverse turbulence intensity (right column). RD (a and b), ELP3_minor (c and d), ELP3_major (e and f).

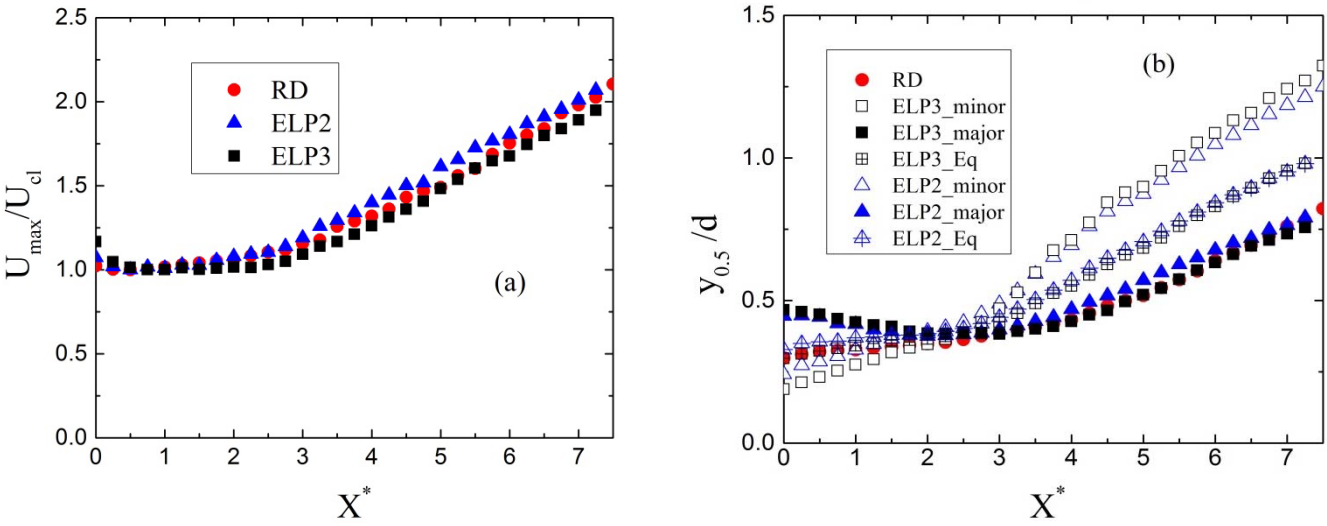

Figure 3: Mean streamwise velocity decay on jet centerline (a) and Half-velocity width (b)

The two-point correlation is employed to characterize the turbulence structure, and quantify the physical sizes of these structures. The two-point correlation function between two streamwise velocity fluctuations $u'(x_r, y_r)$ and $u'(x_r + \Delta x, y_r + \Delta y)$ is defined as follows:

$$R_{uu} = \frac{\overline{u'(x_r,y_r)u'(x_r+\Delta x,y_r+\Delta y)}}{u_{rms}(x_r,y_r)u_{rms}(x_r+\Delta x,y_r+\Delta y)} \quad (2)$$

where the point (x_r, y_r) represents the reference location, Δx and Δy are the spatial separation between the points in streamwise and transverse directions and u_{rms} is the root-mean-square of the velocity fluctuations. Similarly the two-point correlation function between two transverse velocity fluctuations is:

$$R_{vv} = \frac{\overline{v'(x_r,y_r)v'(x_r+\Delta x,y_r+\Delta y)}}{v_{rms}(x_r,y_r)v_{rms}(x_r+\Delta x,y_r+\Delta y)} \quad (3)$$

Figure 5 presents R_{uu} contours in the major plane of ELP2 on the jet centerline at four different streamwise locations: X^* = 2, 4, 6 and 7. In these plots, the contour levels from 0.4 to 1 at 0.1 intervals are shown. The contours at X^* = 2 is circular and small but further downstream, the structures become larger and more stretched in the streamwise direction. The plots at larger streamwise distance from the exit exhibit a higher spatial coherence in the axial direction compared to the transverse one. Shinneeb et al. [9, 10] also observed an increase in the size of structures (with increasing streamwise distance) not only in the near-field region of a round jet but also in the far-field region.

In Figure 6 R_{vv} contours of ELP2 in its major plane at various streamwise directions are shown. The size of the contours increases with streamwise distance from the jet exit as was observed in the case of R_{uu}. However, R_{vv} contours are more correlated in transverse direction (y-axis) rather than in streamwise direction (x-axis), as they are stretched more in the y direction than in the x direction.

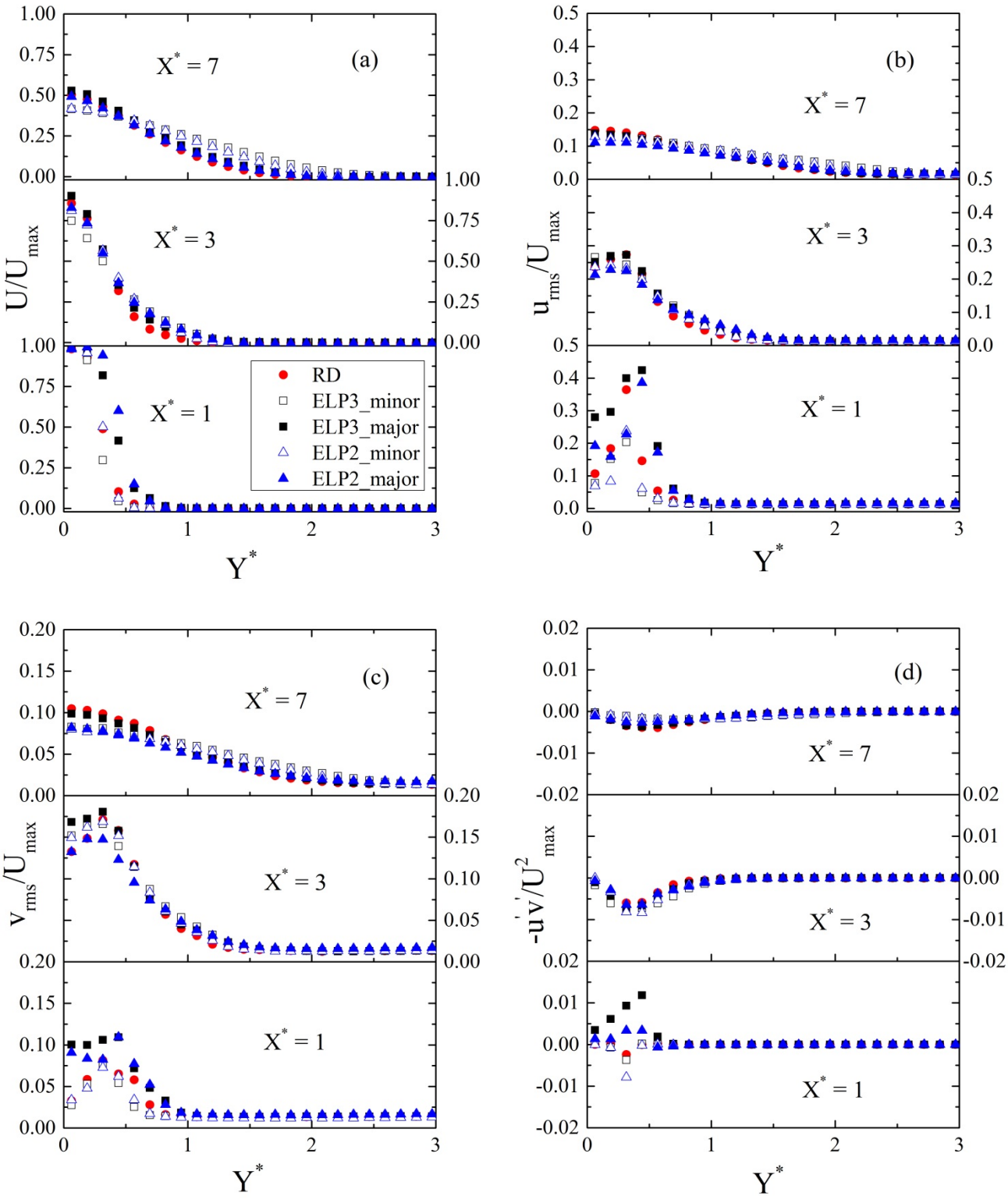

Figure 4: Dimensionless profiles of streamwise mean velocity (a), streamwise turbulence intensity (b), transverse turbulence intensity (c) and Reynolds shear stress (d) at 3 different streamwise locations: X^*= 1, 3 and 7

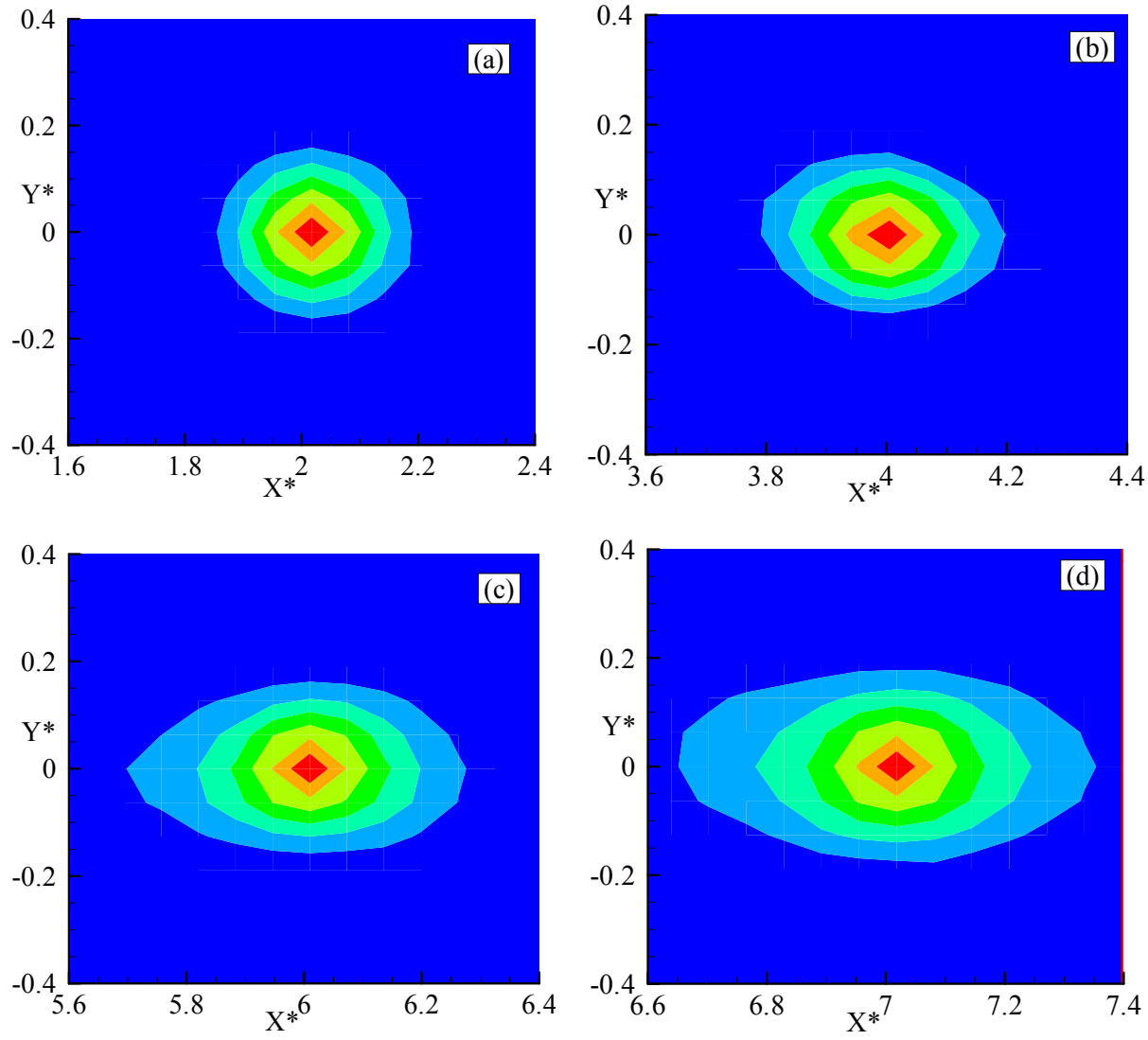

Figure 5: Contours of two point correlation function R_{uu} extracted on the centerline of ELP2 in the major plane at various streamwise locations: $X^* = 2$ (a), $X^* = 4$ (b), $X^* = 6$ (c) and $X^* = 7$ (d). The iso-contours from 0.4 to 1 at 0.1 intervals are shown.

The integral length scales are used to quantitatively compare the physical size of turbulent structures in the different jets (Figure 7). To calculate the integral length scale, first one-dimensional profiles of R_{uu} or R_{vv} were extracted along the x and y directions through the self-correlation points (x_r, y_r), then the resultant integrals are divided by two to obtain the integral length scale. From Figure 7a it is observed that the streamwise integral length scales of R_{uu} (I_{ux}), for all the jets increase with streamwise distance from the jet exit. In addition, ELP3 has the largest integral length scales regardless of streamwise location. Figure 7b presents integral length scales corresponding to R_{vv} in the transverse direction (I_{vy}). The size of structures in RD, ELP2_major and ELP3_major planes increased with streamwise distance while in the minor plane two distinct behaviours are observed: very close to the exit, $X^* < 3$, the structures in the minor planes are larger than in the major plane, and beyond this location the trend is reversed. Figure 7c which corresponds to the transverse integral length scales of R_{uu} (I_{uy}), shows that I_{uy} does not increase with streamwise distance and just fluctuates between 0.13d and 0.23d. Finally the streamwise integral length scales of R_{vv} (I_{vx}) show growth up to the $X^* \leq 2$ but beyond $X^* = 2$, there is no significant change (Figure 7d). The distributions are also independent of nozzle geometry.

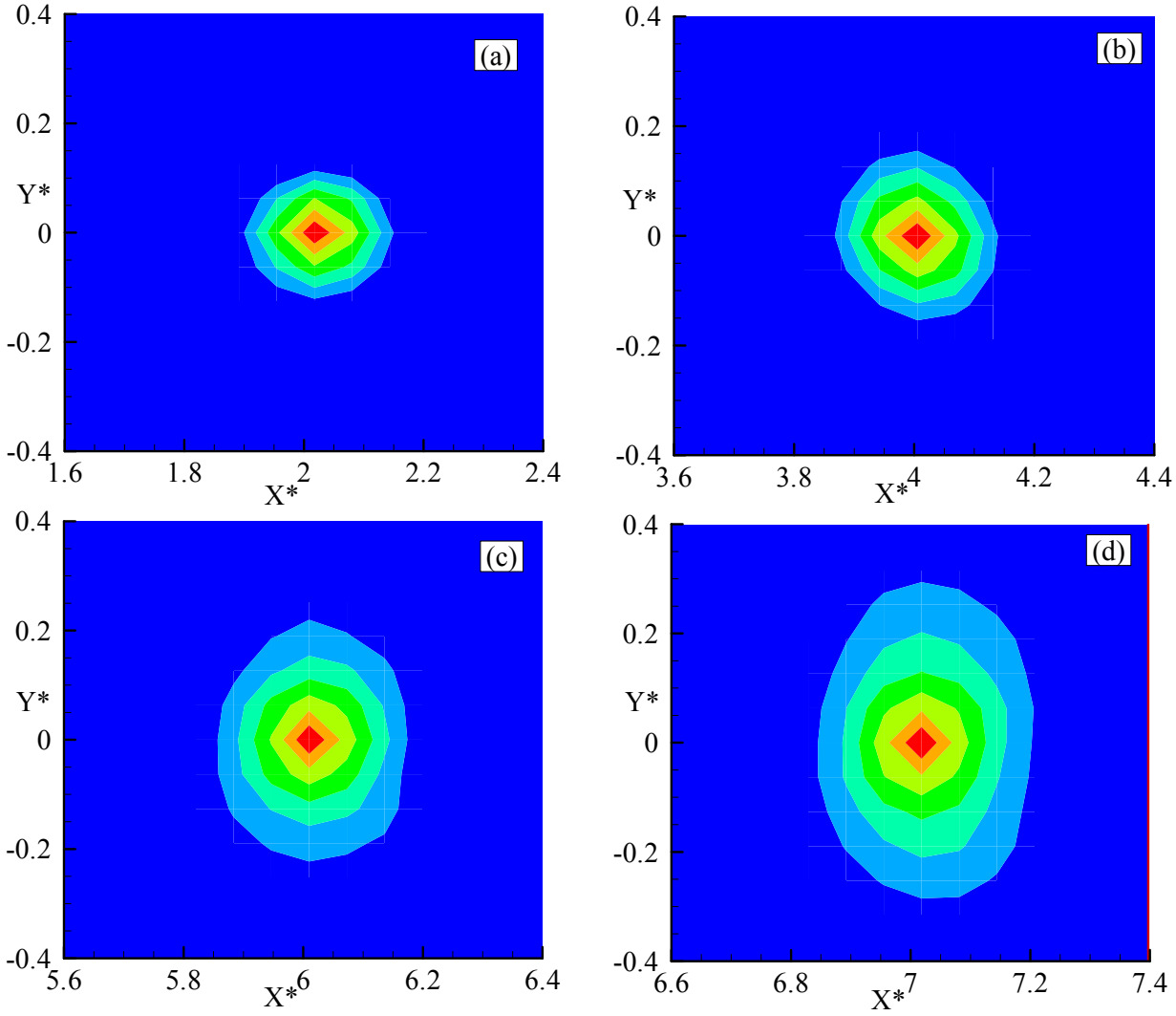

Figure 6: Contours of two point correlation function R_{vv} extracted on the centerline of ELP2 in the major plane at various streamwise locations: $X^* = 2$ (a), $X^* = 4$ (b), $X^* = 6$ (c) and $X^* = 7$ (d). The iso-contours from 0.4 to 1 at 0.1 intervals are shown.

4. Summary and Conclusion

Comprehensive velocity measurements were conducted to investigate the mean velocity as well as turbulence quantities in the near-field region of low Reynolds number free jets produced from round (RD), and elliptic nozzles with aspect ratio 2 (ELP2) and 3 (ELP3) cross-sections. It was observed that ELP3 had the largest spread rate followed by ELP2. In addition to that, asymmetric shape of elliptic nozzles caused the occurrence of different behavior in their minor and major planes, for example, a faster spread rate in minor planes after axis-switching. The axis-switching phenomenon which was present in both ELP2 and ELP3 led to a sign change of Reynolds shear stress in the major planes close to the jet exit. Investigation of the sizes of turbulence structures revealed that they became bigger as the streamwise distance from the jet exit increases.

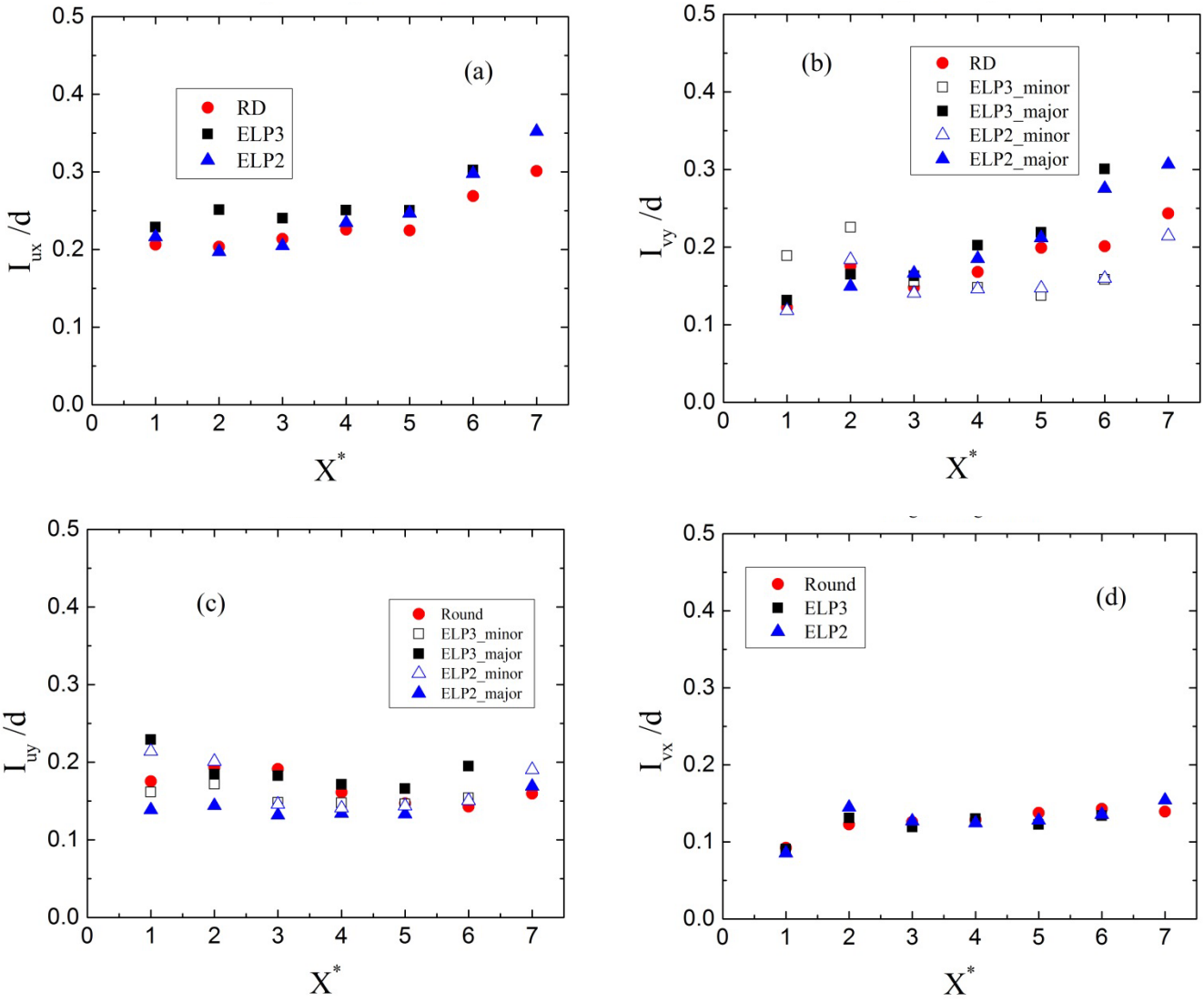

Figure 7: Streamwise integral length scales of R_{uu} (a), Streamwise integral length scales of R_{vv} (b), transverse integral length scales of R_{uu}(c) and transverse integral length scales of R_{vv}(d)

5. References

[1] Abdel-Rahman A (2010) A review of effects of initial and boundary conditions on turbulent jets, *WSEAS TRANSACTIONS on FLUID MECHANICS*, vol. 5(No. 4), pp 257-275.
[2] Mi J, Nathan G J and Nobes D S (2001) Mixing characteristics of axisymmetric free jets from a contoured nozzle, an orifice plate and a pipe, *Journal of Fluid Engineering*, vol. 123, pp 878-883. DOI: 10.1115/1.1412460.
[3] Quinn W R (2006) Upstream nozzle shaping effects on near field flow in round turbulent free jets, *European Journal of Mechanics B/Fluids*, vol. 25, pp 279-301. DOI:10.1016/j.euromechflu.2005.10.002.
[4] Abdel-Rahman A, Al-Fahed S F and Chakroun W (1996) The near-field characteristics of circular jets at low Reynolds numbers, *Mechanic Research Communication*, vol. 23(No. 3), pp 313-324.
[5] Hashiehbaf A and Romano G P (2013) Particle image velocimetry investigation on mixing enhancement of noncircular sharp edge nozzles, *International Journal of Heat and Fluid Flow,* vol. 44, pp 208-221.
[6] Quinn W R (2005) Measurements in the near flow field of an isosceles triangular turbulent free jet, *Experiments in Fluids*, vol. 39, pp 111–126. DOI: 10.1007/s00348-005-0988-2.

[7] Mi J, Nathan G J and Luxton R E (2000) Centerline mixing characteristics of jets from nine differently shaped nozzles, *Experiments in Fluids*, vol. 28, pp 93-94.
[8] Mi J and Nathan G J (2010) Statistical properties of turbulent free jets issuing from nine differently-shaped nozzles, Flow Turbulence Combustion, vol. 84, pp 583-606. DOI: 10.1007/s10494-009-9240-0.
[9] Shinneeb A M, Buggb J D and Balachandarc R (2008) Quantitative investigation of vortical structures in the near-exit region of an axisymmetric turbulent jet, *Journal of Turbulence,* vol. 9(No. 19), pp 1–20. DOI: 10.1080/14685240802195185.
[10] Shinneeb A M, Balachandar R and Bugg J D (2008) Analysis of Coherent Structures in the Far-Field Region of an Axisymmetric Free Jet Identified Using Particle Image Velocimetry and Proper Orthogonal Decomposition, *Journal of Fluids Engineering,* vol. 130. DOI: 10.1115/1.2813137.